Resonances of the $j\ ^3\Delta_g$ state in the differential photodissociation cross section of H_2

L. D. A. Siebbeles, J. M. Schins, and J. Los
FOM–Institute for Atomic and Molecular Physics, Kruislaan 407, 1098 SJ Amsterdam, The Netherlands

M. Glass-Maujean
Laboratoire de Spectroscopie Hertzienne de l'Ecole Normale Supérieure, Université Pierre et Marie Curie, 4 place Jussieu, 75252 Paris CEDEX 05, France

(Received 13 August 1990; revised manuscript received 4 December 1990)

Resonances in the differential photodissociation cross section of H_2 are studied. Photon excitation from the metastable $c\ ^3\Pi_u^-$ state occurs around resonances in the $j\ ^3\Delta_g$ state lying in the continuum of the $i\ ^3\Pi_g$ state. The $j\ ^3\Delta_g$ state is coupled to the continuum by the nuclear rotation. Since direct excitation to the continuum can also occur, interference is present, which expresses itself as a change in anisotropy of the photofragments as the photon energy is scanned over a resonance. Fano parameters, linewidths, and anisotropy parameters are obtained from the measured differential cross sections and are treated theoretically as outlined in the preceding paper [Glass-Maujean and Siebbeles, Phys. Rev. A **44**, 1577 (1991)]. The experimental and calculated results are in good agreement.

I. INTRODUCTION

This paper deals with the photodissociation of H_2 in the metastable $c\ ^3\Pi_u^-$ state by excitation around resonances in the $j\ ^3\Delta_g$ state, which lie in the energy range of the continuum of the $i\ ^3\Pi_g$ state (see Fig. 1). The theory needed to describe such a photodissociation process is presented in the preceding paper [1]. The $j\ ^3\Delta_g$ states are predissociative due to the coupling to the $i\ ^3\Pi_g$ state continuum by the rotational motion of the nuclei. Since both the $j\ ^3\Delta_g$ state and the $i\ ^3\Pi_g$ state carry oscillator strength from the $c\ ^3\Pi_u^-$ state, the total photodissociation cross section as a function of energy has a Beutler-Fano profile [2,3] showing interference effects. Such profiles have been studied earlier in H_2 as a function of energy only [4–10]. The present work deals with the relative photodissociation cross section as a function of both photon energy and angle of dissociation with respect to the laser polarization vector. A preliminary report has been published earlier [11]. For higher absolute values of the Fano asymmetry parameter interference is not easy to observe in the total cross section. The presence of interference is more obvious in the change in anisotropy over the absorption profile. Anisotropy parameters and relative values of coupling matrix elements can be obtained from the measured differential cross sections.

In our method of translational spectroscopy both the released kinetic energy and the angle of dissociation of a molecule can be determined. These observables constitute the differential photodissociation cross section for each specific rovibrational level of the $c\ ^3\Pi_u^-$ state. The so-obtained differential cross sections are used to obtain Fano asymmetry parameters, linewidths, and anisotropy parameters.

This paper has been organized as follows. In Sec. II the theoretical framework to interpret the experimental data is sketched. In the preceding paper [1] a more rigorous treatment of the theory is given. In Sec. III the experimental method is described. In Sec. IV A the total photodissociation signal is discussed and the resonances due to the $j\ ^3\Delta_g$ state are pointed out. The way to use a kinetic energy release spectrum to obtain information on

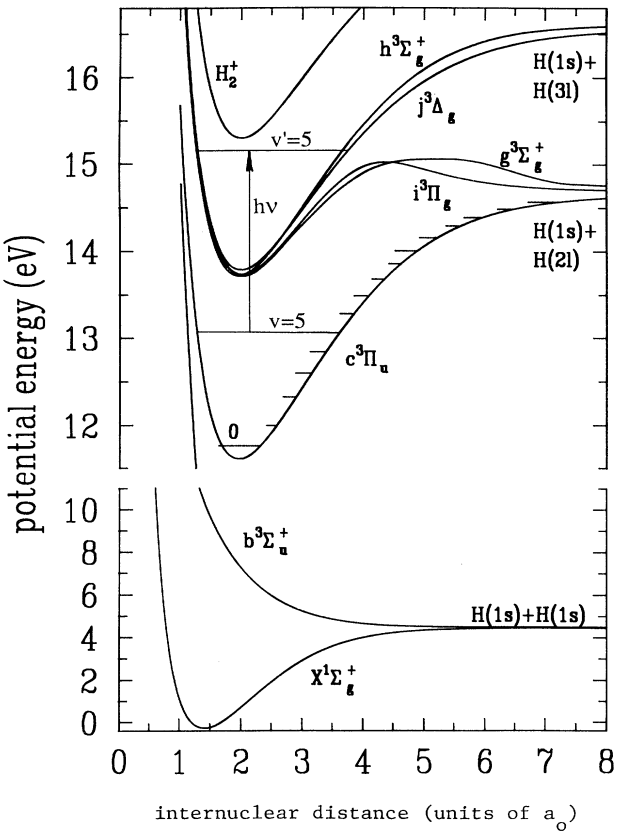

FIG. 1. Relevant potentials of H_2.

the differential photodissociation cross section is presented in Sec. IV B. The differential photodissociation cross sections are presented in Sec. IV C. Linewidths, Fano asymmetry parameters, and anisotropy parameters obtained from the experimental data are also given in Sec. IV C. In Sec. V the experimental values are compared with calculated results. The conclusions are presented in Sec. VI.

II. THEORY

The excited electronic states of H_2 that can be reached from the metastable $c\,^3\Pi_u^-$ state by absorption of a photon with a wavelength near 600 nm are presented in Fig. 1. The $j\,^3\Delta_g$ state and the $i\,^3\Pi_g$ state can very well be described as a $3d\delta$ and a $3d\pi$ state respectively, [12] in Hund's coupling scheme (b) [13] and are coupled by the nuclear rotation. This phenomenon, often called L uncoupling, means a tendency to Hund's case (d). L uncoupling in $n=3$ Rydberg states of H_2 for states lying below the barrier in the $i\,^3\Pi_g$ state has been studied previously [14–17]. In the $g\,^3\Sigma_g^+$ state and the $h\,^3\Sigma_g^+$ state the outer electron has both $3s$ and $3d$ character [15]. These states will also be coupled to the $i\,^3\Pi_g$ state by the rotational motion of the nuclei. The $h\,^3\Sigma_g^+$ resonances are well separated from those of the $j\,^3\Delta_g$ state, thus they do not have to be considered in the photodissociation process. Since excitation to the continuum of the $i\,^3\Pi_g$ state will simultaneously lead to excitation to the continuum of the $g\,^3\Sigma_g^+$ state, the $g\,^3\Sigma_g^+$ state gives rise to a background cross section.

L uncoupling in the $j\,^3\Delta_g$ state is brought into account by introducing the rotational Hamiltonian, which is given by [19]

$$H_R = B(r)\mathbf{R}^2 = B(r)(\mathbf{N}^2+\mathbf{L}^2-2L_z^2-N_+L_--N_-L_+)\,, \tag{2.1}$$

where $B(r)=\hbar^2/2\mu r^2$ with μ the reduced mass and r the internuclear distance. From the presence of the level shift operators in the right-hand expression of Eq. (2.1) it can be seen that H_R only couples electronic states differing by $\Delta\Lambda=\pm1$. Furthermore H_R will couple states with the same electronic wave functions, i.e., the same principal quantum number, same total electronic angular momentum, same inversion symmetry, and having the same parity with respect to reflection in the plane of the nuclear rotation. So the nuclear rotation couples $j\,^3\Delta_g$ rovibrational states only to the $i\,^3\Pi_g$ state.

To obtain an expression for the cross section of the photodissociation process [18], the following molecular states have to be considered: the lower metastable $c\,^3\Pi_u^-(v,N)$ state with vibrational quantum number v and rotational quantum number N, which absorbs a photon, the intermediate predissociative $j\,^3\Delta_g(v',N')$ state giving rise to a resonance, the $i\,^3\Pi_g$ energy normalized continuum state $|\mathbf{k}\rangle$ describing the two hydrogen atoms flying apart with momentum $\hbar\mathbf{k}$, and the analogous $g\,^3\Sigma_g^+$ continuum state.

The total perturbation is $H_R-\mathbf{u}\cdot\mathbf{e}_\lambda$, with $\mathbf{u}$ the dipole moment operator and $\mathbf{e}_\lambda$ the polarization vector of the electromagnetic field. This system is treated theoretically in the preceding paper [1]. The transition moment for excitation from a level in the $c\,^3\Pi_u^-$ state with rotational quantum numbers N and M to the $j\,^3\Delta_g$ state and the $i\,^3\Pi_g$ state simultaneously can be written as

$$\langle\mathbf{k}|T(E)|c\,^3\Pi_u^-(v,N,M)\rangle = \sum_{v',N'}\left[\frac{\langle\mathbf{k}|H_R|j\,^3\Delta_g(v',N',M)\rangle\langle j\,^3\Delta_g(v',N',M)|-\mathbf{u}\cdot\mathbf{e}_\lambda|c\,^3\Pi_u^-(v,N,M)\rangle}{E-E_{v'N'}+\frac{1}{2}i\Gamma_{v'N'}}\right] + \langle\mathbf{k}|-\mathbf{u}\cdot\mathbf{e}_\lambda|c\,^3\Pi_u^-(v,N,M)\rangle\,. \tag{2.2}$$

In Eq. (2.2) $T(E)$ is the reaction operator [18], which defines the final state vector produced by the interaction of the electromagnetic field with the $c\,^3\Pi_u^-$ state. $E_{v'N'}$ is the resonant photon energy for excitation to the predissociative level $j\,^3\Delta_g(v',N')$ with a width $\Gamma_{v'N'}$, which is according to Fano [3] equal to

$$\Gamma_{v'N'}=2\pi|V|^2\,, \tag{2.3a}$$

with

$$V=[N'(N'+1)-\Lambda_j(\Lambda_j-1)]^{1/2}\langle\psi^i_{\Lambda_i}|L_-|\psi^j_{\Lambda_j}\rangle \times\left\langle\chi^i_{\epsilon N'}\left|\frac{-\hbar^2}{2\mu r^2}\right|\chi^j_{v'N'}\right\rangle\,, \tag{2.3b}$$

which is nonzero for $\Lambda_i=\Lambda_j-1$. The electronic wave functions are represented by ψ, while the relative motion of the nuclei is described by the wave functions χ. The matrix element which involves the level shift operator L_- is assumed to be independent of the internuclear separation r.

The first term in the right-hand expression of Eq. (2.2) brings into account the dissociation due to excitation from the $c\,^3\Pi_u^-$ state to predissociative levels in the $j\,^3\Delta_g$ state. The second term corresponds to dissociation by excitation to the continuum of the $i\,^3\Pi_g$ state directly. In the $j\,^3\Delta_g$ state the spacing of the energy levels is large in comparison to their width, so the sum over v',N' in the first term of Eq. (2.2) can be approximated by only the term corresponding to the resonance around which the excitation takes place. As there is no level in the $h\,^3\Sigma_g^+$

state lying close to the selected resonance in the $j\,^3\Delta_g$ state, the contribution of the $h\,^3\Sigma_g^+$ state coupled to the continuum of the $i\,^3\Pi_g$ state to the cross section can be neglected.

The level width Γ given by Eq. (2.3a) depends on the matrix element V of the rotational Hamiltonian H_R, as defined in Eq. (2.1), between the $j\,^3\Delta_g$ state and the $i\,^3\Pi_g$ continuum state. This L-uncoupling matrix element, given in Eq. (2.3b), increases as the rotational quantum number N' goes up. The level width reduces for a larger component Λ_j of the electronic angular momentum on the internuclear axis. This reflects the fact that a larger value of Λ_j implies less nuclear rotation for a fixed value of N' and a stronger coupling to L to the internuclear axis. The smaller nuclear angular momentum implies a reduction of the L uncoupling.

For excitation above the barrier in the $i\,^3\Pi_g$ state the recoil velocity of the hydrogen atoms will be much larger than the rotational velocity, so the axial recoil approximation can be made. For an isotropic distribution of the initial state, taking into account one resonance and making the axial recoil approximation, the differential cross section for photodissociation with linearly polarized light can be written as [1]

$$\frac{d\sigma(E,\Theta)}{d\Omega}=\frac{d\sigma_0(E,\Theta)}{d\Omega}+\frac{d\sigma_g(E,\Theta)}{d\Omega}$$
$$\equiv\frac{A[1+\tilde{\beta}_{\rm res}P_2(\cos\Theta)]}{(E-E_{\rm res})^2+(\Gamma/2)^2}+\frac{2(E-E_{\rm res})B[1+\beta_{\rm int}P_2(\cos\Theta)]}{(E-E_{\rm res})^2+(\Gamma/2)^2}+C(E)[1+\beta_{ci}P_2(\cos\Theta)]+\frac{dg_g(E,\Theta)}{d\Omega}\ . \tag{2.4}$$

E_r is the resonant photon energy for excitation to the predissociative level with a width Γ.

The first term in the last right-hand expression of Eq. (2.4) corresponds mainly to excitation to the resonance, the second term to the interference term, and the third and fourth terms to direct excitation to the continua of the unperturbed $i\,^3\Pi_g$ state and the $g\,^3\Sigma_g^+$ state, respectively. Integrating the differential cross section $d\sigma_0(E,\Theta)/d\Omega$ over all angles yields a Fano-Beutler profile [2,3]

$$\sigma_0=\sigma_a\frac{(E-E_{\rm res}+\Gamma q/2)^2}{(E-E_{\rm res})^2+(\Gamma/2)^2}+\sigma_b\ . \tag{2.5}$$

σ_a is the probability for direct excitation to the interacting continuum, which is the component of the $i\,^3\Pi_g$ continuum state with the same rotational quantum number N as that of the resonance in the $j\,^3\Delta_g$ state. σ_b brings the excitation probability to all noninteracting continua into account. Comparison of Eqs. (2.4) and (2.5) gives

$$A/(\tfrac{1}{2}\Gamma)^2=\sigma_a(q^2-1)=\tilde{\sigma}_{\rm res}\ , \tag{2.6a}$$

$$B/(\tfrac{1}{2}\Gamma)^2=\sigma_a q\ , \tag{2.6b}$$

$$q=\frac{A}{B\Gamma}+\frac{B}{|B|}\left[\left[\frac{A}{B\Gamma}\right]^2+1\right]^{1/2}$$
$$=(-1)^{p'}\frac{M_j}{\pi V M_{i\epsilon}}\frac{\begin{bmatrix}N & 1 & N'\\ \Lambda_c & p' & -\Lambda_j\end{bmatrix}}{\begin{bmatrix}N & 1 & N'\\ \Lambda_c & p & -\Lambda_i\end{bmatrix}}\ , \tag{2.6c}$$

with the properties of the states involved

$$p=\Lambda_i-\Lambda_c=0,\quad p'=\Lambda_j-\Lambda_c=1\ ,$$

and the transition moments

$$M_j=\langle\chi^j_{v'N'}\psi^j_{\Lambda_j}|u_x+u_y|\psi^c_{\Lambda_c}\chi^c_{vN}\rangle\ , \tag{2.6d}$$

$$M_{i\epsilon}=\langle\chi^i_{\epsilon N'}\psi^i_{\Lambda_i}|u_z|\psi^c_{\Lambda_c}\chi^c_{vN}\rangle\ . \tag{2.6e}$$

$M_{i\epsilon}$ is to be compared with the result of Eq. (22) in the preceding paper [1]. The disappearance of the phase factor is due to the application of the axial recoil approximation. In many cases the transition probability for dissociation via the resonance is much larger than that for direct excitation to the continuum, implying that $|q|\gg 1$. In such cases the photodissociation cross section as a function of energy is nearly symmetrical and the following approximate relation can be obtained:

$$q^2\cong\left[\frac{2A}{B\Gamma}\right]^2\cong\frac{\sigma_{\rm res}}{\sigma_a}\ . \tag{2.7}$$

In Eq. (2.7) $\sigma_{\rm res}\cong A/(\frac{1}{2}\Gamma)^2$ corresponds to the dissociation probability by excitation to the resonant state.

The resonance is important over an energy range Γ. Within this range the contribution of the direct excitation to the continua represented by the third and fourth terms in Eq. (2.4) may be considered as independent of E. The background cross section in Eq. (2.4) due to the $g\,^3\Sigma_g^+$ state is given by

$$\frac{d\sigma_g(E,\Theta)}{d\Omega}=\frac{2\pi^2}{3\lambda}M^2_{g\epsilon}[1+\beta_{cg}P_2(\cos\Theta)]\ , \tag{2.8a}$$

with

$$\beta_{cg}=-3(\Lambda_g-\Lambda_c)^2+2=-1\ . \tag{2.8b}$$

Since the last two terms in the right-hand expression of Eq. (2.4), describing the bound-free excitation, have the same energy dependence, their sum can be written as

$$\sigma_{\rm cont}[1+\beta_{\rm cont}P_2(\cos\Theta)]\ ,$$

with

$$\sigma_{\text{cont}}=\sigma_a+\sigma_b=\frac{2\pi^2}{3\lambda}(M_{i\epsilon}^2+M_{g\epsilon}^2) \tag{2.9a}$$

and

$$\beta_{\text{cont}}=\frac{M_{i\epsilon}^2\beta_{ci}+M_{g\epsilon}^2\beta_{cg}}{M_{i\epsilon}^2+M_{g\epsilon}^2} . \tag{2.9b}$$

The photodissociation cross section is asymmetric as a function of photon energy due to the presence of the factor $E-E_r$ in the numerator of the interference term. The change of the sign of this factor as the photon energy is scanned over the resonance also results in a different anisotropy for excitation below or above the resonance. For high values of $|q|$ the occurrence of interference is difficult to detect on the total photodissociation cross section, but manifests itself much more clearly as the change of the anisotropy.

The anisotropy parameters in Eq. (2.4) are derived in the preceding paper [1] and given explicitly for P, Q, and R branches [Eqs. (32) and (33)]. The general expressions of the anisotropy parameters in Eq. (2.4) are

$$\tilde{\beta}_{\text{res}}=\frac{\beta_{\text{res}}(q^2+1)-2\beta_{ci}}{q^2-1} , \tag{2.10a}$$

with

$$\beta_{\text{res}}=5\frac{\begin{pmatrix}2&1&1\\0&0&0\end{pmatrix}\begin{Bmatrix}2&1&1\\N&N'&N'\end{Bmatrix}\begin{pmatrix}N'&N'&2\\\Lambda_i&-\Lambda_i&0\end{pmatrix}}{\begin{pmatrix}0&1&1\\0&0&0\end{pmatrix}\begin{Bmatrix}0&1&1\\N&N'&N'\end{Bmatrix}\begin{pmatrix}N'&N'&0\\\Lambda_i&-\Lambda_i&0\end{pmatrix}} , \tag{2.10b}$$

$$\beta_{\text{int}}=-3(\Lambda_i-\Lambda_c)^2+2=2 , \tag{2.10c}$$

$$\beta_{ci}=-3(\Lambda_i-\Lambda_c)^2+2=2 . \tag{2.10d}$$

The value of the anisotropy parameter in Eq. (2.10d) for direct excitation to the continuum is the value obtained semiclassically within the axial recoil approximation. For a Π-Π transition the electronic transition moment is parallel to the internuclear axis and a $\cos^2\Theta$ distribution of the photofragments is obtained. The anisotropy of the interference term is the same as that for the continuum as can be seen in Eqs. (2.10c) and (2.10d). It must be noted that for a parallel or perpendicular transition, the differential photodissociation cross section for a continuum vanishes at, respectively, $\Theta=90°$ and 0°. In such a direction a predissociation resonance appears without a contribution due to the continuum. The interference term must cancel and so its anisotropy has to be the same as that of the continuum.

III. EXPERIMENT

The relative differential photodissociation cross sections have been measured by means of translational spectroscopy, which has proven to be an excellent tool to investigate dissociative processes [8,16,20]. Both the kinetic energy release (KER) in the center of mass of the molecule and the angle of dissociation with respect to the molecular beam axis can be determined. Figure 2 contains a schematic drawing of the experimental setup.

A 4–6-keV beam of H_2 in the metastable $c\,^3\Pi_u^-$ state is created by charge exchange of H_2^+ in Cs vapor. The ions are extracted from a Nier-type electron-impact source and after mass selection with a Wien filter the H_2^+ beam is focused on the detector. The hydrogen atoms resulting from charge exchange of H_2^+ to dissociative states in H_2 are caught away by a diaphragm behind the charge exchange cell. The remaining H_2^+ ions are removed by a set of deflection plates. Behind the diaphragm the beam of H_2 in the metastable $c\,^3\Pi_u^-$ state is crossed by a tunable intracavity used cw dye laser operated with rhodamine 6G dye. The bandwidth of the laser is 1 cm^{-1} and its polarization vector lies along the molecular beam axis. The fragments resulting from absorption of a photon are detected in coincidence with a time- and position-sensitive detector as described in Ref. [20]. The time and position resolution are better than 1.5 ns and 140 μm, respectively. The KER value ε and the angle of dissociation Θ can be calculated from the determined distance R and time difference of arrival τ of the atoms impinging on the detector. To a very good approximation this can be done according to

$$\varepsilon=\frac{E_0}{4L^2}[R^2+(v_0\tau)^2] , \tag{3.1}$$

$$\Theta=\arctan\left[\frac{R}{v_0\tau}\right] . \tag{3.2}$$

In these equations E_0 is the beam energy, v_0 the beam velocity, and L the flight length from the point of dissociation to the detector. With the mentioned beam energies and a flight length of approximately 2 m KER values from 50 to 1000 meV can be detected. Undissociated molecules are removed by a V-shaped beam flag in order to reduce background signal.

Since for each individual dissociation ε and Θ are determined, data can be accumulated in different ways. A total absorption spectrum of the metastable $c\,^3\Pi_u^-$

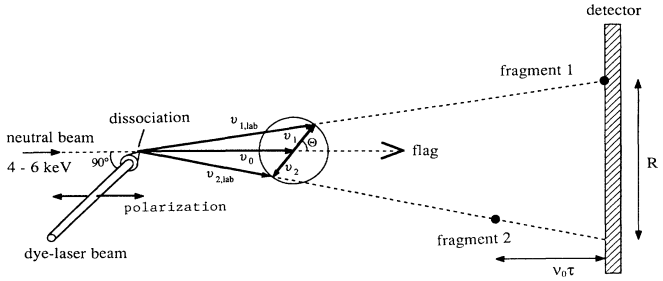

FIG. 2. Schematic representation of the experimental setup. By use of the Newton diagram the kinetic energy release and the dissociation angle Θ can be calculated from the determined distance R and arrival time difference τ.

beam is obtained by measuring the total dissociation rate (irrespective of ε and Θ) as a function of laser wavelength. Such a spectrum is given in Sec. IV A. The photodissociation cross section of a single rovibrational level in the $c\ ^3\Pi_u^-$ state is determined by monitoring the number of counts in the corresponding ε peak in the KER spectra obtained at different laser wavelengths (accumulation time one hour per wavelength). A typical KER spectrum is presented in Sec. IV B. Since both ε and Θ are determined, the angular distribution of the photofragments is thus obtained at definite laser wavelength. Angular spectra are presented in Sec. IV C.

The relative differential photodissociation cross section $d\sigma(E,\Theta)/d\Omega$ for a rovibrational level in the $c\ ^3\Pi_u^-$ state can be obtained by controlling the number of counts N in the corresponding peak in the KER spectra at different dissociation angles Θ, for several photon energies E. In the absence of saturation the number of counts between Θ and $\Theta+\Delta\Theta$ can be approximated by

$$N=\frac{d\sigma(E,\Theta)}{d\Omega}cf(\varepsilon,\Theta)\left[\int V_{\rm int}n_f n_i dt\right](\sin\Theta)\Delta\Theta\,\Delta E\ , \tag{3.3}$$

where the integration takes place over the time during which the measurement takes place. $V_{\rm int}$ is the interaction volume, n_f the photon density per unit of energy, n_i the density of molecules, c the light velocity, ΔE the laser bandwidth and $f(\varepsilon,\Theta)$ the detector efficiency for a KER value ε and dissociation angle Θ. The detector efficiency, which brings into account the position dependence of the sensitivity of the channelplates in the detector, has been determined experimentally. For the determination of the cross section at some photon energy as a function of Θ only, the value of the integral in Eq. (3.3) is not needed, since it appears as a proportionality constant only. However, to obtain the relative cross section as a function of photon energy too, a set of experiments has to be performed and relative values for this integral have to be determined. The integral in Eq. (3.3) is controlled by setting n_i equal to the average value of the number of coincident counts in a unit of time just before and after each measurement without the beam flag and the laser. These coincident count rates, resulting from dissociations due to collisions of H_2 in the metastable $c\ ^3\Pi_u^-$ state on background gas, will be proportional to n_i. A relative value for $\int n_f dt$ is obtained by integrating the output power of the dye laser over the time of the measurement. The overlap between the molecular beam and the laser beam varies smoothly in time. Therefore the time dependence of $V_{\rm int}$ has to be brought into account. This has been done by determining a relative value for the cross section at a reference wavelength with an arbitrary constant value of $V_{\rm int}$. The cross section so obtained can then be used to determine a relative value of $V_{\rm int}$ at any other instant. At the other instant the number of counts N, obtained at the reference wavelength, is determined again. Since the relative value of the cross section had already been determined the relative value of $V_{\rm int}$ at the new instant can be obtained by using Eq. (3.3).

IV. RESULTS

A. Total photodissociation

Recording the total rate of photodissociation of H_2 in the metastable $c\ ^3\Pi_u^-$ state as a function of laser wavelength gives an absorption spectrum as shown in Fig. 3. This dissociation rate is determined as the total count rate of coincidences on the detector, irrespective of the released kinetic energy and the angle at which the two hydrogen atoms fly apart. The signal not induced by the laser, resulting from dissociations of metastable H_2 on background gas, could be subtracted by the use of a chopped laser beam. The dissociation signal is due to simultaneous excitation from several rovibrational levels in the $c\ ^3\Pi_u^-$ state. Excitation can occur to the continua of the $i\ ^3\Pi_g$ and the $g\ ^3\Sigma_g^+$ states, giving rise to a signal which does not depend much on the photon energy, or to a resonance resulting in a peak in the absorption spectrum. Three different types of resonances can be distinguished in the absorption spectrum: broad ones, which are due to predissociation by rotational coupling of levels above the barriers of the $i\ ^3\Pi_g$ and the $g\ ^3\Sigma_g^+$ state; narrow resonances resulting from rotational coupling and subsequent tunneling below the top of these barriers; and thirdly the very sharp peaks due to fluorescence decay to the repulsive $b\ ^3\Sigma_u^+$ state. The width of these sharp peaks indicates the optical resolution of the experiment.

The indication of a peak by, for instance, the notation $i(2,2)R1$ means excitation from $(v=2,N=1)$ in the $c\ ^3\Pi_u^-$ state to $(v=2,N=2)$ in the $i\ ^3\Pi_g^-$ state. The excited states populated by photon absorption, lying below the $H(1s)+H(2l)$ dissociation limit, can decay to the repulsive $b\ ^3\Sigma_u^+$ state by emission of a photon. This is the case for most of the sharper peaks in the absorption spectrum. There are two narrow peaks due to levels with $v=4$ in the $j\ ^3\Delta_g$ state, which lie above the $H(1s)+H(2l)$ dissociation limit, but below the barrier in the $i\ ^3\Pi_g$ state. The small widths of these peaks show that rotational coupling of the $j\ ^3\Delta_g$ state to the $i\ ^3\Pi_g$ state followed by dissociation through barrier tunneling is a relatively slow pro-

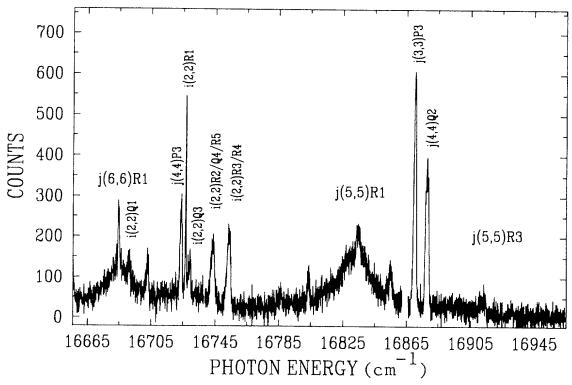

FIG. 3. Spectrum showing the total dissociation rate of H_2 molecules by photon absorption from several rovibrational levels in the metastable $c\ ^3\Pi_u^-$ state. See text for meaning of peak indication.

TABLE I. Experimental and theoretical photon energies E and widths Γ in cm^{-1} for excitation from the $c\,^3\Pi_u^-$ to the $j\,^3\Delta_g^-$ state.

Transition	E_{expt}	E_{theor}	ΔE	Γ_{expt}	Γ_{theor}
$j(5,5)R1$	16 833±1	16 829	4	23±1	24
$j(5,5)R3$	16 920±3	16 903	17	98±7	96
$j(6,6)R1$	16 685±1	16 682	3	19±1	18
$j(7,7)R1$	16 538±2	16 536	2	16±1[a]	17
$j(8,8)R1$		16 389			15

[a]In Ref. [10] a value of 29±1 cm^{-1}, obtained by use of a double-resonance technique, is reported.

cess. Excitation to levels with $v \geq 5$ in the $j\,^3\Delta_g$ state gives rise to the broader structures in the absorption spectrum. Since these levels lie above the barrier in the $i\,^3\Pi_g$ state, the rotation couples them directly to the $i\,^3\Pi_g$ continuum, resulting in a shorter lifetime. An absorption spectrum gives information on both positions and widths of resonances (see Table I).

B. Kinetic energy release spectra

If the laser wavelength is fixed, a KER spectrum as shown in Fig. 4 can be obtained. The KER spectrum has been taken for a dissociation angle between 88° and 90° with respect to the laser polarization vector, which gives the best energy resolution. The peaks in this spectrum are due to excitation from various rovibrational levels in the $c\,^3\Pi_u^-$ state, so the distances between the peaks reflect the energy differences between the corresponding rovibrational levels of the $c\,^3\Pi_u^-$ state, which are characterized by a vibrational quantum number v and a rotational quantum number N. In the energy range below 1.0 eV, the peaks in the KER spectrum result from dissociation of the molecule to the $H(1s)+H(2l)$ dissociation limit.

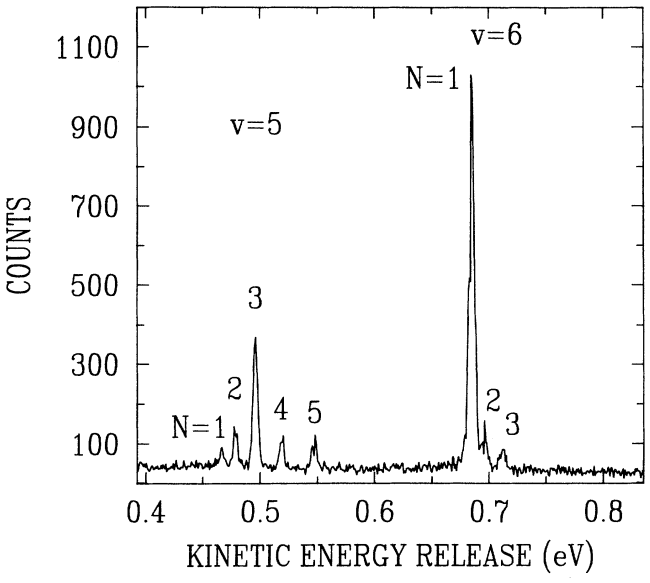

FIG. 4. Kinetic energy release spectrum taken at a fixed photon energy of 16 699 cm^{-1}, showing peaks due to photodissociation from rovibrational levels of the $c\,^3\Pi_u^-$ state.

The relative intensities of the KER peaks are partly determined by the populations of the lower levels, but also by the presence of resonances, to which excitation can occur. These resonances make the relative intensities of the KER peaks change as the photon energy is varied. In Fig. 4 the high intensity of the $(v=6,N=1)$ peak at a photon energy of 16 699 cm^{-1} results from an R-branch-like excitation close to the $(v=6,N=2)$ level in the $j\,^3\Delta_g^-$ state. The intensity of the $(v=5,N=1)$ peak is even smaller than those belonging to the less populated $(v=5,N=2,3)$ levels in the $c\,^3\Pi_u^-$ state. The $(v=5,N=1)$ peak will be dominated by direct excitation to the $i\,^3\Pi_g$ and $g\,^3\Sigma_g^+$ continua, while for $N=2,3$ resonances also contribute to the photodissociation cross sections. The KER spectra can thus be used to study resonances in the cross section for photodissociation of the metastable H_2 molecules.

C. Differential photodissociation cross section

1. *Isotropy of $c\,^3\Pi_u^-$ state*

Throughout the paper it is assumed that the $c\,^3\Pi_u^-$ state is populated isotropically. In order to test this, the angular distribution for excitation to the very sharp resonance due to $(v=4,N=2)$ in the $j\,^3\Delta_g^-$ state, reached by the $J(4,4)R1$ transition, has been investigated. The $j\,^3\Delta_g^-$ state with $(v=4,N=2)$ gives rise to a sharp resonance because it dissociates relatively slowly by tunneling through the $i\,^3\Pi_g^-$ state barrier. At this energy no resonance is present in the $i\,^3\Pi_g$ state and so the dissociation process can be described as slow predissociation described by Beswick and Durup [21]. The angular part of the photodissociation cross section for this transition can be written as

$$\frac{d\sigma(\Theta)}{d\Omega} = P_{M=0}\left(\tfrac{2}{15}+\tfrac{2}{21}D_{00}^2(\Theta)-\tfrac{8}{175}D_{00}^4(\Theta)\right) + P_{|M|=1}\left(\tfrac{1}{5}+\tfrac{1}{14}D_{00}^2(\Theta)+\tfrac{8}{175}D_{00}^4(\Theta)\right) . \quad (4.1)$$

The Wigner matrix elements $D_{00}^2(\Theta)$ and $D_{00}^4(\Theta)$ are defined in Ref. [19]. The right-hand expression of Eq. (4.1) has been fitted to the experimental cross section with the populations P_M as parameters. It turned out that the populations of the different M sublevels of the lower state are equal to within 3%. From this it was concluded that the charge exchange process results in an isotropic beam

of H_2 in the $c\ ^3\Pi_u^-$ state.

After having shown that the $c\ ^3\Pi_u^-$ state is populated isotropically in the charge exchange process, the relative differential photodissociation cross sections will be analyzed in Secs. IV C 2 and IV C 3.

2. *Energy dependence of the photodissociation cross section*

In Fig. 5 relative photodissociation cross sections are plotted as a function of photon energy at a dissociation angle between 88° and 90° with respect to the laser polarization vector. The points are experimental results, obtained from the KER spectra. The solid curves are the result of a least-squares fit of the expression in Eq. (2.4) with the substitution of the last two terms by Eqs. (2.9a) and (2.9b) to the experimentally obtained relative differential cross sections at different photon energies. From the energy dependence of the photodissociation cross section near 90° only the resonant excitation energy E_r and the level width Γ can be obtained. From the angular dependence, which is discussed in the next section, in combination with the energy dependence of the photodissociation cross section the Fano asymmetry parameter and the anisotropy parameters of the different terms in Eq. (2.4) can be determined. The results obtained by the

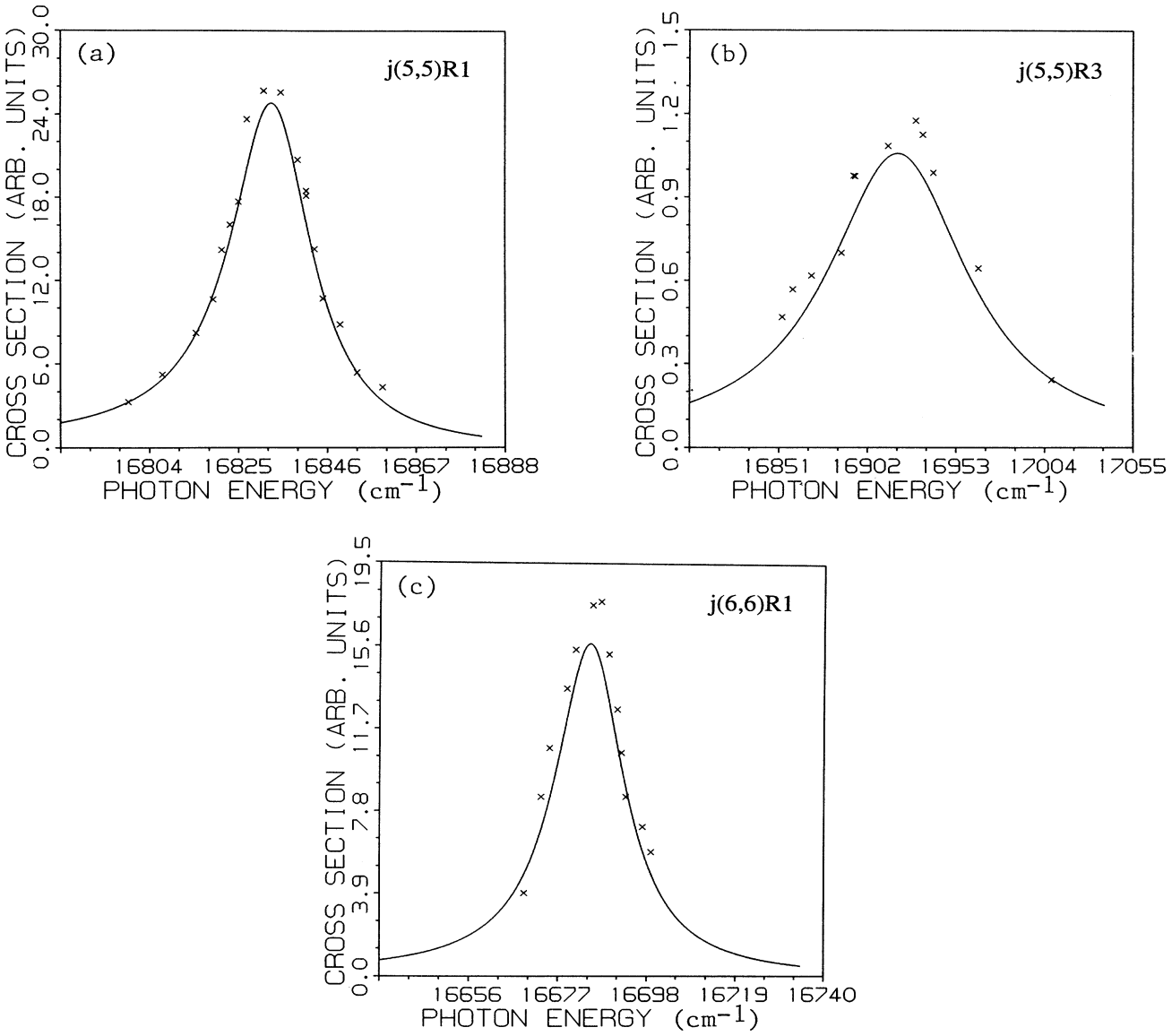

FIG. 5. Relative photodissociation cross sections for transitions as indicated in the figures as function of photon energy for a dissociation angle $\Theta = 90°$. The crosses are experimental points and the curves result from a least-squares fit. As is pointed out in Sec. IV C 2, the fitted curves have been obtained by a fitting procedure as a function of both photon energy and dissociation angle. Due to electronic crosstalk in the detector the values at $\Theta = 90°$ are relatively high and therefore the fit might seem to be unoptimized.

TABLE II. Experimental and theoretical Fano asymmetry parameters. The values marked with an asterisk have been taken from Ref. [10].

Transition	q_{expt}	q_{theor}
$j(5,5)R1$	$-16(+1,-12)$	-13
$j(5,5)R3$	$-4(+1,-4)$	-5
$j(6,6)R1$	$-14(+2,-19)$	-16
$j(7,7)R1$		-17
$j(8,8)R1$	-16 ± 3*	-18
$j(12,12)R1$	-11 ± 3*	-26
$j(10,11)R1$	-13 ± 2*	-14

least-squares-fitting procedures for three lower levels in the $c\,^3\Pi_u^-$ state, with A, B, σ_{cont}, Γ, E_r, $\bar{B}_r$, β_i, and β_{cont} as adjustable parameters, are presented in Tables I–IV.

In Figs. 5(a)–5(c) and 6 the relative error in the experimental points is mainly determined by the stability of the laser and particle beams [Eq. (3.3)] and is estimated to be about 10%. As will be seen in Sec. IV C 3, the angular profiles systematically exhibit small wiggles, due to electronic crosstalk in the detector. For example, all profiles display a maximum at 90°. Since the least-squares-fit procedure optimizes with respect to the complete angular profiles and energy dependence of the cross section, an apparent mismatch results in Fig. 5 where only the fit at $\Theta=90°$ is shown. The statistical error in the spectra is less than 1%. The relative weak intensity of the $N=2$ peak [at most 10% for the $j(5,5)R1$ transition] ensures that the error due to partial overlap of the $N=2$ peak with the $N=1$ peak is less than 5%.

As indicated in Fig. 5, excitation by R branches occurs around, respectively, ($v=5,N=2$), ($v=5,N=4$), and ($v=6,N=2$) in the $j\,^3\Delta_g^-$ state. The level widths obtained from these data are in principle more accurate than those from the absorption spectrum in Fig. 3, because in Fig. 3 the signal is due to simultaneous excitation from several rovibrational levels in the $c\,^3\Pi_u^-$ state instead of only from the one of interest. The importance of having the KER spectra can be appreciated from the structure due to the ($v=5,N=4$) resonance [Fig. 5(b)]. This resonance is extremely weak, so it cannot be distinguished in the total absorption spectrum of Fig. 3. Comparison of Figs. 5(a) and 5(b) shows that the level width Γ of the profile increases as the rotational quantum number goes up. This is due to the stronger rotational interaction or L uncoupling for a higher rotational quantum number. From Figs. 5(a) and 5(c) it can be seen that the width is smaller for a higher vibrational quantum number, which has also been observed on the $3p\pi\ ^1\Pi_u$ profiles [7]. In Table I the experimental widths are given together with calculated ones. Lembo *et al.* [10] have performed double resonance experiments on the higher-lying vibrational levels in the $j\,^3\Delta_g$ state. To allow a direct comparison to the data of Lembo *et al.* [10] the width of the ($v=7,N=2$) resonance in the $j\,^3\Delta_g^-$ state has been measured from the total photodissociation signal in the absorption spectrum in Fig. 7. The sharp structure near 16 538 cm^{-1} is assigned to the $i(2,2)P2$ transition.

TABLE III. Ratios of background and resonant cross sections.

	$\sigma_{\text{cont}}/\sigma_{\text{res}}$	
Transition	Expt.	Theor.
$j(5,5)R1$	$(5\pm3)\times10^{-2}$	1.3×10^{-2}
$j(5,5)R3$	0.24 ± 0.24	0.1
$j(6,6)R1$	$(5\pm5)\times10^{-2}$	0.01

Note that according to Eq. (2.9b) $\beta_{\text{int}}=\beta_{ci}=2$ for transitions from the $c\,^3\Pi_u^-$ state to the $i\,^3\Pi_g$ state. Thus the second and third terms in Eq. (2.4) are proportional to $\cos^2\Theta$, which is zero at $\Theta=90°$. At this angle there is no interference and the profiles should by symmetric, which is observed (see Fig. 5). At the magic angle (about 55°) the shape of the energy dependence of the cross section is equal to that of the total, angle integrated, cross section. The asymmetry in the total cross section, determined by the q parameter, is illustrated in the magic angle (Θ between 54° and 56°) spectrum for the $j(5,5)R1$ transition (Fig. 6). The symmetric profile at $\Theta=90°$ is given for comparison.

By use of the second right-hand expression in Eq. (2.6c) values of q can be obtained from the results of the fitting procedures. The absolute value of q for the $j(5,5)R3$ transition is small in comparison to that for the $j(5,5)R1$ transition. According to Eq. (2.7) a higher rotational quantum number thus results in the decrease of the dissociation probability via the resonance in comparison to direct dissociation. From the q values in Table II it is seen that dissociation via the resonance is relatively more important for $v=6$ than for $v=5$, which will be partly due to the reduction of the level width for a higher vibrational quantum number.

3. *Angular dependence of photodissociation cross section*

The angular dependence of the photodissociation cross sections is shown in Figs. 8–10 for R branches and a Q branch, respectively. These figures reflect the angular dependence of the intensity of a peak in the KER spectrum obtained at a fixed laser wavelength. It is shown that the angular dependence of a Fano profile is not the same in each point. The present experiments by which the change of the angular dependence with photon energy is probed are much more sensitive to the occurrence of interference than measurements of the total cross section. As was already pointed out in the preceding section, the measured angular dependence of the cross sections allowed us to determine Fano asymmetry parameters and anisotropy parameters.

As has been pointed out in the preceding section, the wiggles in the angular profiles are due to electronic crosstalk of the detector. Note the systematic behavior of this effect in Fig. 8, where maxima can be seen at practically the same angles for all angular profiles. The relative error in the signal resulting from statistical noise and partial overlap of peaks in the KER spectre is estimated

TABLE IV. Experimental and theoretical anisotropy parameters.

	Experimental			Theoretical		
Transition	$\tilde{\beta}_{res}$	β_{int}	β_{cont}	$\tilde{\beta}_{res}$	β_{int}	β_{cont}
$j(5,5)R1$	0.5±0.05	1.3±0.3	1.7±0.3	0.48	2.0	1.5
$j(5,5)R3$	0.9±0.3	1.7±0.3	1.7±0.3	0.47	2.0	1.5
$j(5,5)Q3$	−0.71±0.05[a]			−0.90		
$j(6,6)R1$	0.6±0.05	1.7±0.3	1.7±0.3	0.49	2.0	1.4

[a]For this transition a photon energy of 16 730 cm^{-1} has been used, which is resonant according to Ref. [16].

to be smaller than 6%. In Fig. 8 the experimentally obtained angular dependence of the cross section is presented for different photon energies close to the resonant energy of, respectively, the $j(5,5)R1$, the $j(5,5)R3$, and the $j(6,6)R1$ transition. As can be seen from Fig. 5(a) and Table I, the profile at 16 835 cm^{-1} in Fig. 8(a) is almost at the resonant photon energy, while the two other profiles in Fig. 8(a) are almost one level width below and above the resonant energy. At these energies the relative contribution of the resonance is weaker, making the influence of the continuum of the $i\,^3\Pi_g$ state more important. From Fig. 5(a) it is seen that the height of the latter two profiles at $\Theta=90°$ is about one-third of the one on resonance. In Fig. 8 the profiles are scaled to coincide at $\Theta=90°$, in order to make the comparison of their shapes easier.

It is clear from Fig. 8 that for each transition the shape of the angular profiles changes as the photon energy is varied. This will be partly due to the fact that changing the photon energy alters the relative contribution of the probability of dissociation via the resonance [first term in Eq. (2.4)] and that for direct dissociation [last two terms in Eq. (2.4)]. But if this were the only reason for the difference, the profiles would be the same at equal energies below and above the resonance, since the difference of the photon energy and the energy of the resonance appears quadratically in the denominator of the first term in Eq. (2.4). In Fig. 8(a) the profiles at 16 815 and 16 853 cm^{-1} are at nearly equal distance below and above the resonant excitation energy. The difference of their shape only results from the occurrence of interference. The interference term in Eq. (2.4), which contains the factor $E-E_{res}$ in the numerator, appears with opposite sign below and above the resonant energy. So the angular dependence of the cross section is different for excitation below or above the resonance.

As can be seen from Eq. (2.4) subtraction of the photodissociation cross section below the resonant photon energy from that at equal energy above the resonance yields the interference term. The result of subtracting the curve at 16 815 cm^{-1} from that at 16 853 cm^{-1} (these curves are to within the experimental error at equal distance

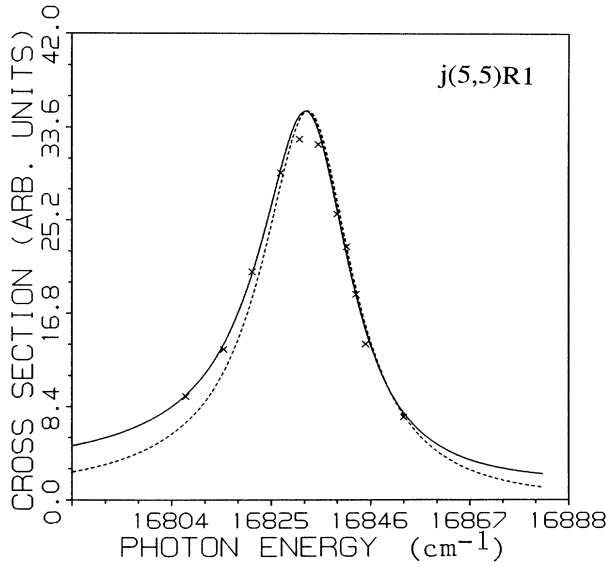

FIG. 6. Relative photodissociation cross sections as function of photon energy for $j(5,5)R1$ transition. The crosses are experimental points for a dissociation angle Θ near the magic angle, while the solid curve is the result of a least-squares fit for this angle as explained in the text. The dashed curve is the result of the fit at $\Theta=90°$.

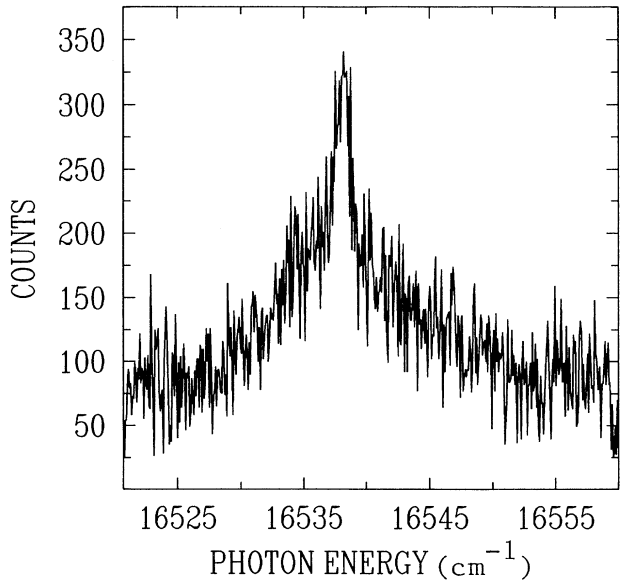

FIG. 7. Spectrum showing photodissociation rate of the metastable H_2 beam for photon energies around the resonant energy for the $j(7,7)R1$ transition. The sharp peak near 16 538 cm^{-1} is assigned to the $i(2,2)P2$ transition.

from the resonance) is presented in Fig. 9. Since according to Eq. (2.9b) the anisotropy of the interference term is such that no interference occurs for a dissociation angle of 90°, the two curves at 16 815 and 16 853 cm^{-1} should coincide at $\Theta = 90°$. Therefore the curves at 16 815 and 16 853 cm^{-1} have been scaled accordingly before subtraction. Figure 9 clearly shows that the magnitude of the interference term is important and increases at smaller dissociation angles. The sign of the interference term is in agreement with the calculated one as described in Sec. V.

The off-resonant profiles in Fig. 8(c) for the $j(6,6)R1$ transition at 16 675 and 16 693 cm^{-1} are about half the level width away from the resonant energy at 16 685 cm^{-1}. Although the influence of interference on the profiles is now somewhat less strong, they show the same behavior as those for the $j(5,5)R1$ transition. The reduction of the importance of interference conforms to the somewhat larger absolute value of q for the $j(6,6)R1$ transition. From Eq. (2.6c) it is seen that for given rotational quantum numbers the variation of q with vibrational quantum number is determined by $M_j/VM_{i\epsilon}$. The increase of the absolute value of q going from $j(5,5)R1$ to the $j(6,6)R1$ transition is, apart from the reduction of V, to a large extent due to an increase of the ratio $M_j/M_{i\epsilon}$. From Eqs. (2.2) and (2.4) it is seen that the terms taking into account the dissociation via the reso-

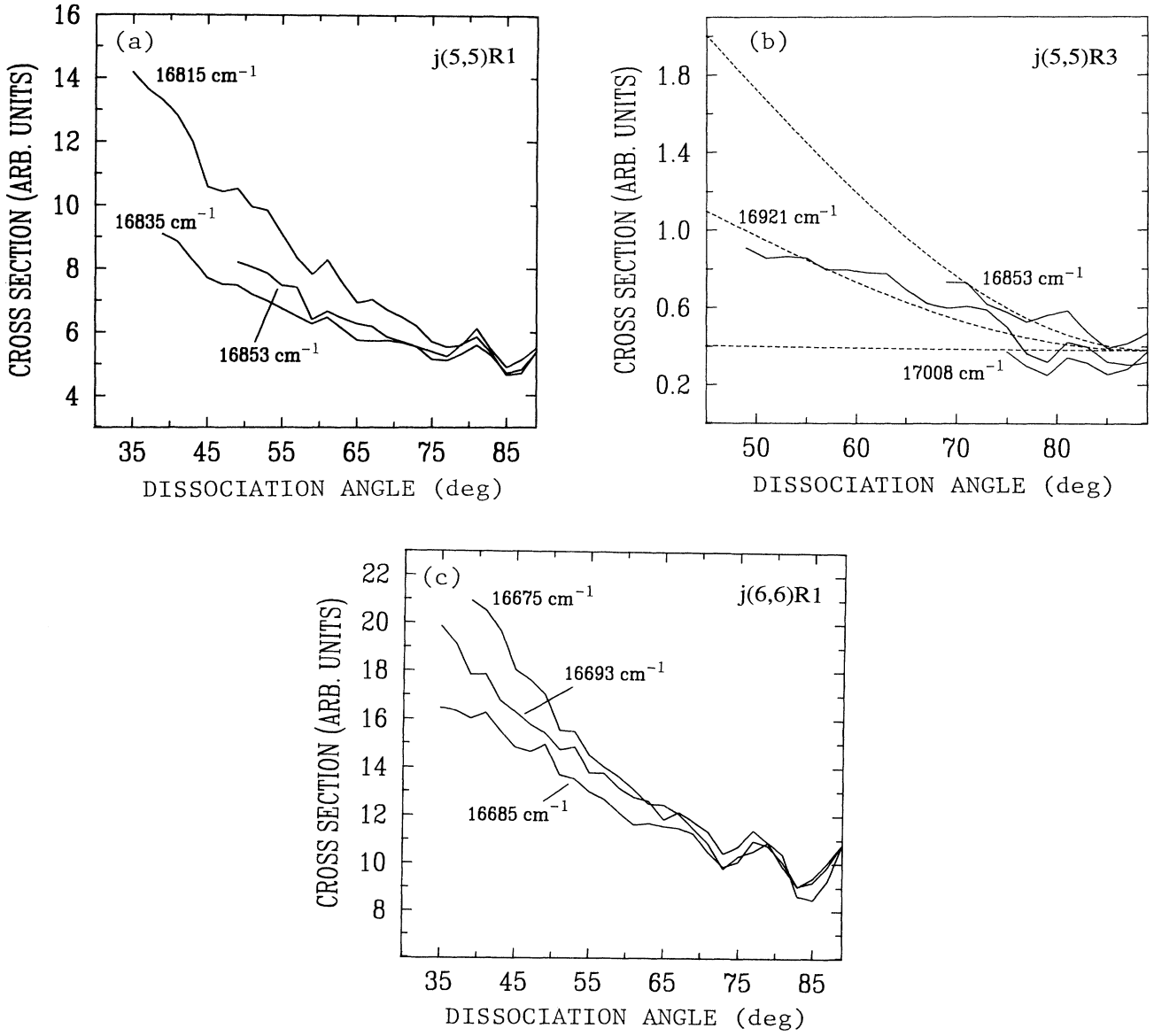

FIG. 8. Relative photodissociation cross sections as function of dissociation angle at photon energies as indicated. In (a)–(c) the photon energies are close to, respectively, the resonant energies for the $j(5,5)R1$, the $j(5,5)R3$, and the $j(6,6)R1$ transition. For each transition the profiles are scaled to coincide at a dissociation angle of 90°. The dashed curves in (b) result from a fit.

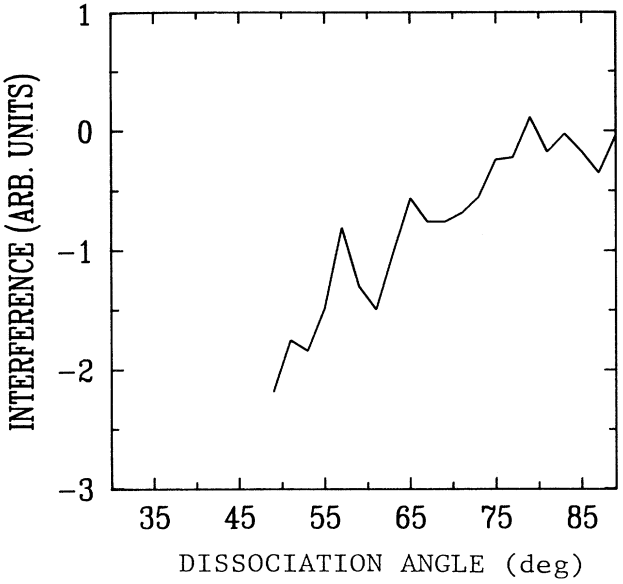

FIG. 9. Angular dependence of interference term of the $j(5,5)R1$ transition, obtained by subtracting scaled profiles at 16 819 and 16 853 cm^{-1}.

nance become relatively more important. The larger contribution of the first term on the right-hand side of Eq. (2.4) reduces the influence of the interference term (second term). This causes the anisotropy to change less as the photon energy is changed from the resonant excitation energy to that at half maximum.

Results for the $j(5,5)R3$ transition can be found in Fig. 8(b). The dashed curves have been obtained by a least-squares-fitting procedure. The curves have been scaled such that those from the fitting procedures coincide at $\Theta=90°$. The fitted curve at 17 008 cm^{-1} lies somewhat above the experimental curve at this photon energy, reflecting the experimental error in the determination of the total cross section.

In Fig. 8(b) the profiles at 16 853 and 17 008 cm^{-1}, being nearly one level width away from the $j(5,5)R3$ resonant transition energy, differ much more from that on resonance at 16 921 cm^{-1} than those for the $j(5,5)R1$ transition. This reflects the relative weakness of the excitation probability of the resonance for the $j(5,5)R3$ transition in comparison to the probability for excitation to the continuum directly, or equivalently, the smaller absolute value of q. The decrease of the first term in Eq. (2.4) due to the resonance is a consequence of the larger width Γ for a higher rotational quantum number. Interference is now more apparent, because the probability for dissociation via the predissociative level differs less from that for direct dissociation. The major importance of interference for the $j(5,5)R3$ transition can be seen as a larger difference in shape of the off-resonant profiles in Fig. 8(b).

The angular dependence of the photodissociation cross section at the resonant excitation energy of 16 730 cm^{-1} (see Ref. [16]) for the $j(5,5)Q3$ transition is presented in Fig. 10. The dashed curve has been obtained by a least-squares fit of $\sigma[1+\beta P_2(\cos\Theta)]$ to the experimental curve with σ and β as adjustable parameters. The so-obtained anisotropy parameter is given in Table IV. The shape of the profile for this Q transition really differs from those of the R transitions. In contrast to the R transitions the cross section at resonance for a Q transition increases with dissociation angle.

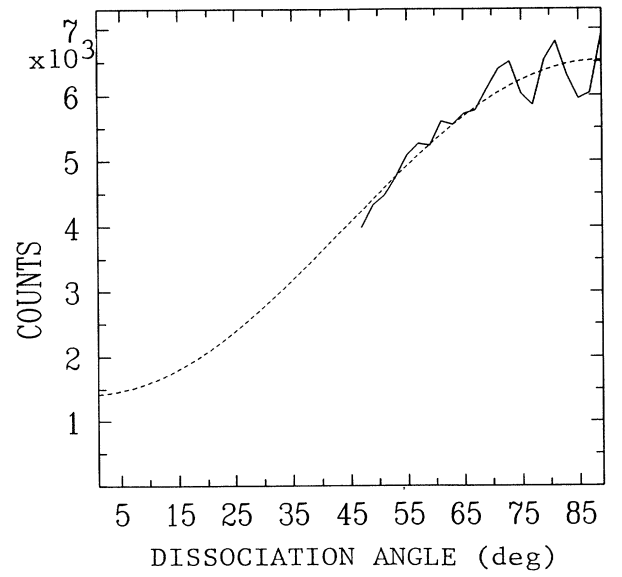

FIG. 10. Angular dependence of the photodissociation cross section at the resonant photon energy for the $j(5,5)Q3$ transition. The dashed curve results from a fit.

V. COMPARISON WITH CALCULATED VALUES

H_2 is theoretically well known and most of the dynamical parameters can be calculated *ab initio*. The potential curves of the $c\,^3\Pi_u$, $i\,^3\Pi_g$, and the $j\,^3\Delta_g$ states of interest here have been calculated by Kolos and Rychlewski [22] and Rychlewski [23], corrected in Ref. [10]. The experimental results in Tables I–IV have been obtained by fitting procedures as described in the first part of Sec. IV C 2.

The energies of rovibronic levels in the $c\,^3\Pi_u$ state and the $j\,^3\Delta_g$ state have been calculated in the Born-Oppenheimer approximation by a Numerov integration method, and used to find the transition energies. The experimental and calculated resonant photon energies E are presented in Table I. For the $R1$ transitions the calculated resonant photon energies are in very good agreement. The $j(5,5)R3$ transition lies 17 cm^{-1} higher than the calculated value, which may be due to an accidental perturbation. The predissociation widths Γ have been calculated from Eq. (2.3) in a pure precession model [24], i.e., considering the $j\,^3\Delta_g$ and the $i\,^3\Pi_g$ states as pure $3d$ states. This approximation has given quite good results in H_2 for the predissociation width of the $3p\pi\ D\,^1\Pi_u$ levels [9,24]. The calculated level widths can be found in the last column of Table I. The agreement with experiment is striking. Lembo *et al.* [10] also measured many level

widths for ($v=7-14, N'=2$) levels in the $j\,^3\Delta_g$ state. However, as they have noted, their widths exceed the calculated values by 30%. It cannot be excluded [27], that power broadening has influenced the widths given in Ref. [10]. Lembo *et al.* [10] also calculated the level widths and their calculated value for the $j(7,7)R1$ transition agrees with the present results.

To calculate the Fano asymmetry parameters q the electronic transition moments between the $c\,^3\Pi_u$ and $j\,^3\Delta_g$, and the $c\,^3\Pi_u$ and $i\,^3\Pi_g$ states are needed. Recently, these transition moments have become available [28]. The relation between the electronic transition moments at the equilibrium internuclear distance (2.0 bohr) is given by [28]

$$\langle \psi^j_{\Lambda_j} | u_x + u_y | \psi^c_{\Lambda_c} \rangle = -1.09 \langle \psi^i_{\Lambda_i} | u_z | \psi^c_{\Lambda_c} \rangle \ . \tag{5.1}$$

The resulting calculated q parameters are presented in Table II. They agree with the experimental values. The sign of q is determined by the sign of B in Eq. (2.6c). B corresponds to the magnitude of the interference term [see Eq. (2.4)]. The calculated negative sign of the q values is in accordance with the sign of the observed interference term shown in Fig. 9. Apart from the $j(12,12)R1$ transition the experimental q parameters of Lembo *et al.* [10] agree very well with the calculated results reported here.

The experimental anisotropy parameters for the R transitions are given in Table IV, together with those calculated by use of Eqs. (2.10), (2.9b), (5.1), and (5.2). For the $R1$ transitions the experimental values of the anisotropy parameter $\tilde{\beta}_{\rm res}$ of the resonant term in Eq. (2.4) are in good agreement with those from the theory. For the $j(5,5)R3$ transition the theoretical value of $\tilde{\beta}_{\rm res}$ lies just outside the estimated error interval of the experimental value. The anisotropy parameter of the resonant term for the $j(5,5)Q3$ transition is, according to Eq. (2.10a), equal to -0.81. This is close to the experimental value, obtained at an excitation energy of 16 730 $\rm cm^{-1}$ and a fit as described in the last paragraph of Sec. IV C 3, which is contaminated by a contribution due to direct excitation to the continua. From the very small difference between the experimental and theoretical values of the anisotropy parameter it turns out that the contribution of the continua to the cross section must be relatively small for resonant excitation.

The experimental anisotropy parameters $\beta_{\rm int}$ of the interference term are in agreement with the theoretical values obtained from Eq. (2.10c), except for the $j(5,5)R1$ transition. It is not clear what the origin of this discrepancy is.

From the experiments the anisotropy parameters $\beta_{\rm cont}$ due to the direct excitation to the continua of the $i\,^3\Pi_g$ and the $g\,^3\Sigma_g^+$ state have been obtained with reasonably sized uncertainty. Theoretical values of $\beta_{\rm cont}$ in Table IV have been estimated by the use of Eqs. (2.9b) and (5.2). The transition probability for excitation to the $g\,^3\Sigma_g^+$ state has been calculated using potential values of Rychlewski [26] and treating the $g\,^3\Sigma_g^+$ state as a pure $3d$ state, which means [25]

$$\langle \psi^g_{\Lambda_g} | u_x + u_y | \psi^c_{\Lambda_c} \rangle = -1/\sqrt{3} \langle \psi^i_{\Lambda_i} | u_z | \psi^c_{\Lambda_c} \rangle \ . \tag{5.2}$$

The experimental and calculated ratios of the bound-free cross section $\sigma_{\rm cont}$ in Eq. (2.9a) and the cross section at resonance $\sigma_{\rm res} \cong A/(\frac{1}{2}\Gamma)^2$ [see Eq. (2.7)], which is due to the resonance, are given in Table III. The weakness of the bound-free transition strength explains the relatively large experimental error. There is, except for the $j(5,5)R1$ transition, no disagreement between experiment and theory. An experiment more sensitive for determination of the differential cross section for direct excitation to the continua of the $i\,^3\Pi_g$ and the $g\,^3\Sigma_g^+$ states is needed to make a proper comparison between experiment and theory possible.

VI. CONCLUSIONS

Fast-beam photofragment spectroscopy can be used to obtain differential photodissociation cross sections. The effect of L uncoupling between the $j\,^3\Delta_g$ state and the $i\,^3\Pi_g$ state of H_2 has been observed. The width of the investigated resonances in the $j\,^3\Delta_g^-$ state increases as the rotational quantum number goes up, reflecting the increase of L uncoupling for higher rotation of the molecule. The calculated widths are completely in agreement with those found experimentally.

The occurrence of interference, due to the fact that the $i\,^3\Pi_g$ state can also be reached directly by photon absorption, appears as an asymmetry in the total photodissociation cross section as a function of energy. The experimental and calculated Fano asymmetry parameters are in good agreement. Besides the relative magnitude of the coupling matrix elements their relative signs, which determine the sign of the Fano parameter, have also been obtained and are fully in agreement with the calculated results.

Although the occurrence of interference also appears as an asymmetry in the total photodissociation cross section as a function of energy only, the role of interference is shown to be apparent in the angular dependence. The observed angular dependence of the cross section clearly shows the expected interference effects. The experimentally obtained anisotropy of the photofragment distribution is in agreement with theory.

ACKNOWLEDGMENTS

Dr. W. J. van der Zande is greatly acknowledged for critically reading the manuscript and many stimulating discussions. R. Brilman is thanked for his technical assistance. This work is part of the research program of the Stichting voor Fundamenteel Onderzoek der Materie (Foundation for the Fundamental Research on Matter) and was made possible by the financial support of the Nederlandse Organisatie voor Wetenschappelijk Onderzoek (Netherlands Organization for the Advancement of Research). The Laboratorie de Spectroscopie Hertzienne is "Unité Associée au Centre National de la Recherche Scientifique No. 18."

[1] M. Glass-Maujean, L. D. A. Siebbeles, preceding paper, Phys. Rev. A **44**, 1577 (1991).
[2] U. Fano, Nuovo Cimento **12**, 56 (1935).
[3] U. Fano, Phys. Rev. **124**, 1866 (1961).
[4] H. Beutler, A. Deubner, H. O. Jünger, Z. Phys. **98**, 181 (1935).
[5] F. J. Comes and G. Schumpe, Z. Naturforsch. Teil A **26**, 538 (1971).
[6] M. Glass-Maujean, J. Breton, and P. M. Guyon, Chem. Phys. Lett. **63**, 591 (1979).
[7] M. Glass-Maujean, P. M. Guyon, and J. Breton, Phys. Rev. A **33**, 346 (1986).
[8] H. Helm, D. P. de Bruijn, and J. Los, Phys. Rev. Lett. **53**, 1642 (1984); D. P. de Bruijn and H. Helm, Phys. Rev. A **34**, 3855 (1986).
[9] J. A. Beswick and M. Glass-Maujean, Phys. Rev. A **35**, 3339 (1987).
[10] L. J. Lembo, D. L. Huestis, S. R. Keiding, N. Bjerre, and H. Helm, Phys. Rev. A **38**, 3447 (1988).
[11] L. D. A. Siebbeles, J. M. Schins, and J. Los, Phys. Rev. Lett. **46**, 1514 (1990).
[12] R. Jost, M. Lombardi, R. S. Freund, and T. A. Miller, Mol. Phys. **37**, 1605 (1979).
[13] G. Herzberg, *Molecular Spectra and Molecular Structure. I. Spectra of Diatomic Molecules* (Van Nostrand Reinhold, New York, 1950).
[14] M. L. Ginter, J. Chem. Phys. **46**, 3687 (1967).
[15] C. B. Wakefield and E. R. Davidson, J. Chem. Phys. **43**, 834 (1965).
[16] W. Koot, W. J. van der Zande, and J. Los, Phys. Rev. A **39**, 590 (1989).
[17] S. R. Keiding and N. Bjerre, J. Chem. Phys. **87**, 3321 (1987)
[18] S. Mukamel and J. Jortner, Chem. Phys. Lett. **29**, 169 (1974).
[19] R. N. Zare, *Angular Momentum* (Wiley, New York, 1988).
[20] D. P. de Bruijn and J. Los, Rev. Sci. Instrum. **53**, 1020 (1982).
[21] P. Glorieux, D. Lecler, and R. Vetter, *Chemical Photophysics* (Centre National de la Recherche Scientifique, Paris, 1979), Chap. F.
[22] W. Kolos and J. Rychlewski, J. Mol. Spectrosc. **66**, 428 (1977).
[23] J. Rychlewski, J. Mol. Spectrosc. **104**, 253 (1984).
[24] F. Fiquet-Fayard and O. Gallais, Mol. Phys. **20**, 527 (1971).
[25] J. T. Hougen, *The Calculation of Rotational Energy Levels and Rotational Line Intensities in Diatomic Molecules* (National Bureau of Standards, Washington, DC, 1970).
[26] J. Rychlewski (private communication).
[27] H. Helm (private communication).
[28] J. M. Schins, L. D. A. Siebbeles, W. J. van der Zande, J. Los, H. Koch, and J. Rychlewski, Phys. Rev. A (to be published).